ISSN 0036-0236, Russian Journal of Inorganic Chemistry, 2019, Vol. 64, No. 2, pp. 170–178. © Pleiades Publishing, Ltd., 2019.
Russian Text © V.I. Pet'kov, D.A. Lavrenov, M.V. Sukhanov, A.M. Koval'skii, E.Yu. Borovikova, 2019, published in Zhurnal Neorganicheskoi Khimii, 2019, Vol. 64, No. 2, pp. 137–145.

SYNTHESIS AND PROPERTIES OF INORGANIC COMPOUNDS

Sol–Gel Synthesis and Structure Formation of Manganese Zirconium (Titanium) Phosphates

V. I. Pet'kov[a], *, D. A. Lavrenov[a], M. V. Sukhanov[a], A. M. Koval'skii[b], and E. Yu. Borovikova[c]

[a] *National Research Nizhny Novgorod State University, Nizhny Novgorod, 603950 Russia*
[b] *National Research and Technology University "MISiS", Moscow, 119049 Russia*
[c] *Moscow State University, Moscow, 119991 Russia*
**e-mail: petkov@inbox.ru*

Received March 20, 2018; revised April 23, 2018; accepted July 6, 2018

Abstract—Compounds $Mn_{0.5}Ti_2(PO_4)_3$ and $Mn_{0.5}Zr_2(PO_4)_3$ and $Mn_{0.5+2x}Zr_{2-x}(PO_4)_3$ ($0 < x \le 0.35$) solid solution were prepared by two variants of the sol–gel method using inorganic and organic reagents and were characterized using X-ray diffraction and IR spectroscopy. $Mn_{0.5}Ti_2(PO_4)_3$, a compound with an $NaZr_2(PO_4)_3$ (NZP) structure, is formed at 600°C and is stable up to 950°C. $Mn_{0.5}Zr_2(PO_4)_3$ has dimorphism; its low-temperature phase having the $Sc_2(WO_4)_3$ (SW) structure was prepared at 650°C, and the high-temperature NZP phase, at 1200°C. $Mn_{0.5+2x}Zr_{2-x}(PO_4)_3$ solid solution crystallizes in an SW-type structure; it is thermally unstable at temperatures above 900°C. The thermal stability of samples decays as x rises. The numbers of the stretching and bending vibrations in an PO_4^{3-} ion in the IR spectra of NZP and SW orthophosphates agree with factor-group analysis for space group $R\bar{3}$ and $P2_1/n$. Structure refinement was carried out for the low-temperature $Mn_{0.5}Zr_2(PO_4)_3$ phase (space group $P2_1/n$, a = 8.861(3) Å, b = 8.869(2) Å, c = 12.561(3) Å, β = 89.51(2)°) and for the solid solution. The basis of the structures is a framework built of corner-sharing tetrahedra PO_4 and octahedra ZrO_6 or $(Mn,Zr)O_6$. The framework interstices are occupied by cations Mn^{2+} in tetrahedral oxygen coordination. A comparative crystal-chemical analysis of the morphotropic series of $M_{0.5}Zr_2(PO_4)_3$ phosphates (M stands for a metal in the oxidation state +2) elucidated a relationship between structural features.

Keywords: phosphates, manganese, zirconium, titanium, sodium zirconium phosphate and scandium tungstate structures, phase formation

DOI: 10.1134/S0036023619020165

INTRODUCTION

Phosphates of formula unit $M_{0.5}E_2(PO_4)_3$ (where M stands for a metal in the oxidation state +2; E = Ti or Zr) belong to the $NaZr_2(PO_4)_3$ (NZP, NASICON) and $Sc_2(WO_4)_3$ (SW) structural types [1, 2]. In both structures the basis is the framework $\{[E_2(PO_4)_3]^{p-}\}_{3\infty}$ built of columns of octahedral-tetrahedral moieties EO_6 and PO_4. The interstices in both structures are occupied by cations of elements in the oxidation state +2. Extensive cationic isomorphism of extraframework cations in NZP and SW type structures and an option of isomorphic substitutions in framework-forming octahedra and tetrahedra determine the large extents of the crystallization fields of compounds $M_{0.5}E_2(PO_4)_3$ and their base solid solutions.

The $M_{0.5}Ti_2(PO_4)_3$ phosphates whose framework is built on the titanium basis (titanium having a smaller size than zirconium), crystallize in NZP structure (Table 1). The $M_{0.5}Zr_2(PO_4)_3$ phosphates with large M^{2+} ions (Cd, Pb, Sr, or Ba) crystallize in the NZP structural type, those with smaller M^{2+} ions sizes crystallize in SW structural type. $Mn_{0.5}Zr_2(PO_4)_3$ has dimorphism and exists as SW and NZP phases. The reported values of the monoclinic-to-tetragonal transition temperature [16, 29] are considerably differing from one another (900–1400°C). The structure of the low-temperature $Mn_{0.5}Zr_2(PO_4)_3$ phase has not been solved.

The $M_{0.5}E_2(PO_4)_3$ compounds have high chemical, thermal, and radiation stability and low thermal expansion [4, 15, 26, 30, 31], and they can be prepared by solid-phase chemical methods or by precipitation from aqueous solutions (sol–gel or hydrothermal synthesis). The incorporation of 3*d* ions (in particular, Mn) into such phosphates made it possible to manufacture promising phosphors and catalysts for dehydrogenation and dehydration of alcohols, isomerization of alkanes, and their selective oxidation [7, 18, 31–35].

Table 1. Structural types of $M_{0.5}E_2(PO_4)_3$ phosphates (M stands for cations in the oxidation state +2, and E stands for Ti, Zr)

Phosphate	Structural type	Space group	Source
$M_{0.5}Ti_2(PO_4)_3$ M = Ni, Mg, Cu, Zn, Co, Fe, Mn, Ca, Sr, Pb, Ba	NZP	$R\bar{3}c$, $R\bar{3}$, $R32$, $R3$	[3–15]
$M_{0.5}Ti_2(PO_4)_3$ M = Cu, Zn	SW	$P2_1/n$	[16, 17]
$M_{0.5}Zr_2(PO_4)_3$ M = Mn, Cd, Ca, Sr, Pb, Ba	NZP	$R\bar{3}c$, $R\bar{3}$	[2, 18–24]
$M_{0.5}Zr_2(PO_4)_3$ M = Ni, Mg, Cu, Co, Zn, Mn	SW	$P2_1/n$	[1, 25–28]

Our goals in this work were to prepare $Mn_{0.5+2x}E_{2-x}(PO_4)_3$ (E = Ti, Zr) phosphates, to study their phase formation, to refine their structures; and to elucidate the concentration and temperature stability fields of solid solutions.

EXPERIMENTAL

The $Mn_{0.5+2x}E_{2-x}(PO_4)_3$ (E = Ti, Zr) samples with x = 0, 0.10, 0.25, 0.35, 0.50, 0.60, 0.75, and 1.0 were prepared by the sol–gel method followed by heat treatment. The initial reagents for the synthesis were chemically pure grade chemicals: $Mn(CH_3COO)_2 \cdot 4H_2O$, $TiOCl_2$ (prepared from $TiCl_3$ via oxidation in air by hydrochloric acid + nitric acid mixture), $ZrOCl_2 \cdot 8H_2O$, and H_3PO_4. Stoichiometric amounts of 1 M aqueous solutions of manganese acetate and titanium or zirconium oxychloride were poured together under constant stirring at room temperature. Then, orthophosphoric acid solution was added under stirring, also in agreement with the stoichiometry. Reaction mixtures were dried at 90°C and then heat-treated under air at 600–1100°C for 24 h at every step. Stepwise heating was alternated with dispersion for homogenization of mixtures. The Pechini citrate method, another version of the sol–gel process, was also used to prepare phosphates. The organic reagents used were citric acid (monohydrate, a chemically pure grade sample) and ethylene glycol (a pure for analysis grade sample), taken in an excess for stable chelate complexes to be formed. To a citric acid solution, solutions of manganese and zirconium (titanium) salts were added, then ammonium dihydrophosphate solution and ethylene glycol were. The resulting samples were dried, dispersed, and stepwise annealed at 90, 130, 350, and 600–950°C. The Pechini method provided a uniform distribution of ions over the polymeric gel and made it possible to reduce the temperature at which single-phase products can be obtained compared to the sol–gel process where organic reagents are not used. The thus-prepared samples were white polycrystalline powders.

The X-ray diffraction patterns of samples were recorded on a Shimadzu XRD-6000 diffractometer (CuK_α radiation, λ = 1.54178 Å, 2θ = 10°–60°). X-ray powder diffraction was used to determine the phase composition of samples in the course of their preparation after every isothermal anneal step and to monitor their phase composition. The X-ray diffraction patterns were indexed by structural analogy using crystallographic data for compounds described in the literature. The unit cell parameters of the prepared phosphates were refined by the least-squares method.

The chemical composition and homogeneity of phosphates were monitored using a JEOL JSM-7600F scanning electron microscope equipped with a thermal field emission electron gun (Schottky cathode). The microscope was equipped with a microanalytical system (an OXFORD X-Max 80 (Premium) energy-dispersive spectrometer with a silicon-drift semiconductor detector). The error in elemental compositions was within 2 at %.

The X-ray diffraction spectra of $Mn_{0.5}Zr_2(PO_4)_3$ (x = 0) and $MnZr_{1.75}(PO_4)_3$ (x = 0.25) samples for structural studies were recorded in the range 2θ = 10°–110° with a 0.02° scan step and an exposure time per point of 16 s. X-ray diffraction patterns were processed and phosphate structures were refined by the Rietveld method [36] in software RIETAN-97 [37]. Peak profiles were fitted by the modified pseudo-Voigt function (Mod-TCH pV [38]). The model used for phosphate structure refinement was the $LiZr_2(AsO_4)_3$ atomic coordinates [39].

The functional composition of samples was verified by IR-spectroscopic studies. IR absorption spectra were recorded on a Shimadzu FTIR-8400S FT-IR spectrometer in the wavenumber range 400–1400 cm^{-1}.

RESULTS AND DISCUSSION

When phase formation in $Mn_{0.5+2x}E_{2-x}P_3O_{12}$ (E = Ti, Zr) was studied, the samples in the course of synthesis were isothermally annealed at 600, 700, 800, and 900°C. The exposure time at every temperature was 24 h. At the end of every step, some samples were rapidly air-quenched and then analyzed, while the others continued to be heated up.

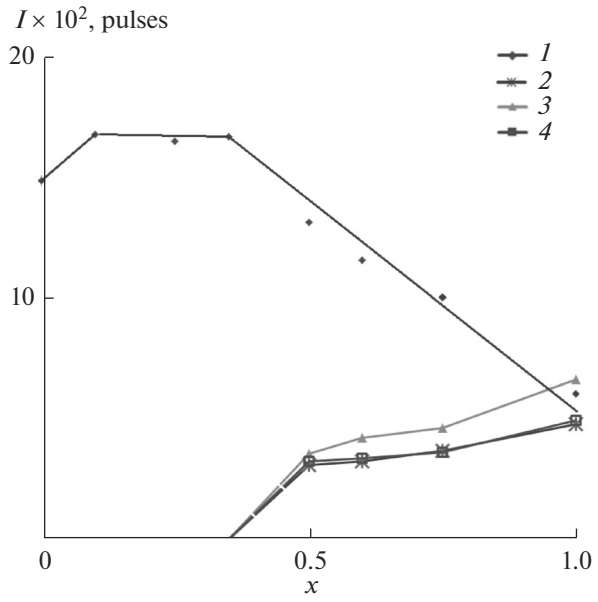

Fig. 1. Strongest reflection intensities versus x for $Mn_{0.5+2x}Zr_{2-x}P_3O_{12}$ samples (synthesis temperature: 650°C). Phase notations: (*1*) $Mn_{0.5+2x}Zr_{2-x}(PO_4)_3$ ($0 \le x \le 0.35$, $2\theta \approx 20°$), (*2*) ZrP_2O_7 ($2\theta = 21.5°$), (*3*) ZrO_2 ($2\theta = 27.5°$), and (*4*) $Mn_2P_2O_7$ ($2\theta = 30.2°$).

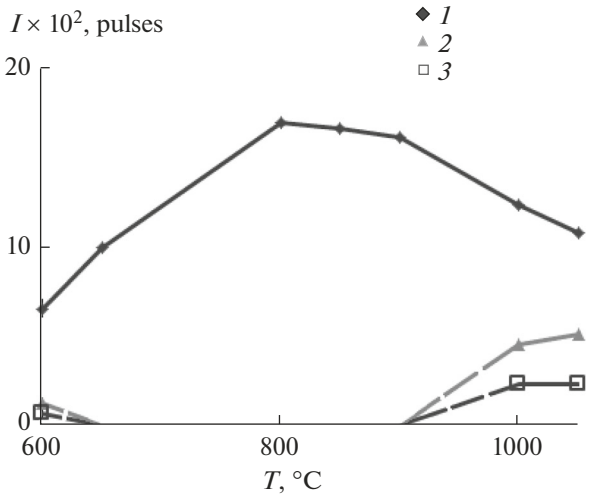

Fig. 2. Strongest reflection intensities versus temperature for the phases that are formed in the $Mn_{0.5}Zr_2(PO_4)_3$ synthesis: (*1*) $Mn_{0.5+2x}Zr_{2-x}(PO_4)_3$ ($0 \le x \le 0.35$, $2\theta \approx 20°$), (*2*) ZrO_2 ($2\theta = 27.5°$), and (*3*) $Mn_2P_2O_7$ ($2\theta = 30.2°$).

A comprehensive study of phase formation in $Mn_{0.5+2x}Ti_{2-x}P_3O_{12}$ showed that the double phosphate $Mn_{0.5}Ti_2(PO_4)_3$ ($x = 0$), as probed by X-ray powder diffraction, is formed at 600°C, crystallizes in rhombohedral system (space group $R\bar{3}$, $a = 8.513(1)$ Å, $c = 21.008(1)$ Å, $V = 1318.5(4)$ Å^3, $Z = 6$), belongs to the NZP structural type, and is stable up to 950°C. The $Mn_{0.5}Ti_2(PO_4)_3$ structure was determined by X-ray structural analysis of hydrothermally prepared single-crystals [9]. Solid solution $Mn_{0.5+2x}Ti_{2-x}(PO_4)_3$ is not formed because of considerable differences between the ionic radii of Ti^{4+} (0.61 Å) and Mn^{2+} (0.83 Å). The results of X-ray powder diffraction studies of the prepared $Mn_{0.5+2x}Zr_{2-x}P_3O_{12}$ samples indicate that their phase compositions depend appreciably on the synthetic method, heat treatment, and the manganese content of the phosphate. The Pechini citrate method enabled us to reduce the temperature at which single-phase products can be obtained compared to the sol–gel process without organic reagents. Figure 1 exemplifies the strongest reflection intensities of phases in $Mn_{0.5+2x}Zr_{2-x}P_3O_{12}$ samples prepared by the Pechini method at 650°C. In the range $x = 0-0.35$, the conditions are for $Mn_{0.5+2x}Zr_{2-x}(PO_4)_3$ solid solution with the SW structure to be formed. The $0.5 \le x \le 1$ samples were mixtures of phases (Fig. 1).

The effect of temperature on the formation of expected solid solution for a phase of composition $Mn_{0.5}Zr_2P_3O_{12}$ ($x = 0$) is shown in Fig. 2 (the exposure time at set temperatures was 24 h). At 600°C X-ray powder diffraction detects a mixture of phases: the desired product, ZrO_2, and pyrophosphate $Mn_2P_2O_7$. Single-phase $Mn_{0.5}Zr_2(PO_4)_3$ is formed at 650°C. As the temperature rises, the crystallinity of the desired phase improves to reach the maximal value at 800–850°C. Above 900°C the temperature-induced phase transition occurs in manganese zirconium phosphate from the monoclinic to rhombohedral structure, accompanied by a partial decomposition of the desired product. A rise in temperature to 1200°C and a long-term heat treatment of the sample at this temperature yielded $Mn_{0.5}Zr_2(PO_4)_3$ with the NZP structure (space group $R\bar{3}$, $a = 8.85(1)$ Å, $c = 21.80(5)$ Å, $V = 1478(4)$ Å^3, $Z = 6$). The structure of the high-temperature $Mn_{0.5}Zr_2(PO_4)_3$ phase was refined by the Rietveld method previously [18].

The samples of prepared individual phosphates and solid solutions were homogeneous as probed by electron microscopy; their chemical compositions according to microprobe analyses corresponded to theoretical values. Figure 3 shows a micrograph of $Mn_{1.0}Zr_{1.75}(PO_4)_3$ ($Mn_{0.5+2x}Zr_{2-x}(PO_4)_3$, $x = 0.25$) by the way of example. The image implies that the grain sizes are differentiated and range from 10 to 100 μm. Microprobe data showed a homogeneous grain composition; chemical analysis corresponded to the formula unit $Mn_{1.00(2)}Zr_{1.75(3)}P_{3.0(1)}O_{12}$.

The X-ray diffraction patterns of $Mn_{0.5+2x}Zr_{2-x}(PO_4)_3$ ($0 \le x \le 0.35$) solid solution samples, which are crystallized in the SW structural type, feature a smooth shift of diffraction peaks with a systematic change in their relative intensities in response to increasing x (Fig. 4). The unit cell parameters a, b, c, and β of $Mn_{0.5+2x}Zr_{2-x}(PO_4)_3$ solid solutions as func-

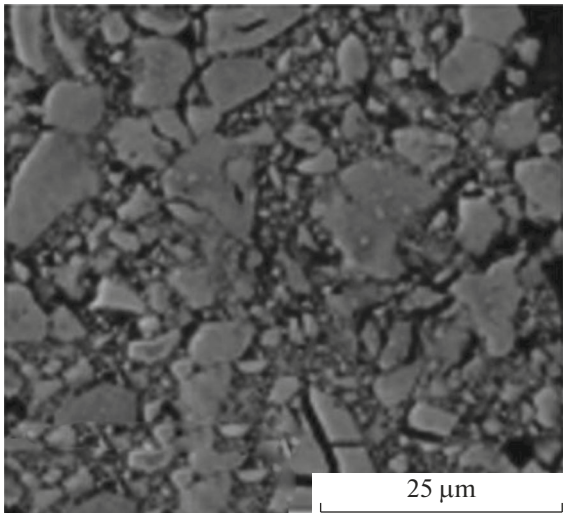

Fig. 3. Micrograph of sample $Mn_{1.0}Zr_{1.75}(PO_4)_3$ (x = 0.25).

tions of x are fitted by the following equations: a = 8.859 – 0.04x (±0.003 Å), b = 8.959 + 0.0531x (±0.006 Å), c = 12.526 + 0.0366x (±0.005 Å), and β = 89.79 – 0.0405x (±0.05°). The crystal-chemical formula of the solid solution, where different crystallographic positions are occupied by manganese cations, with great probability will be the following: $Mn_{0.5 + x}[Mn_xZr_{2 - x}(PO_4)_3]_{3\infty}$, where $[Mn_xZr_{2 - x}(PO_4)_3]_{3\infty}$ stands for the framework in which Mn and Zr occupy positions with CN = 6 and $Mn_{0.5 + x}$ stands for extra-framework positions partially occupied by Mn (CN = 4). The solid solution is thermally unstable at temperatures above 900°C; the thermal stability of samples decreases with rising x.

The IR spectra of individual phosphates and the solid solutions have a pattern typical of orthophosphates with NZP and SW structures with space group $R\bar{3}$ and $P2_1/n$, respectively (Fig. 5). Due to the differing degrees of distortion of PO_4 tetrahedra in the structures of these phosphates, the IR regions of their vibrational spectra differ from one another in the numbers and types of bands in the stretching and bending ranges.

In rhombohedral phosphates (space group $R\bar{3}$), the selection rules for IR spectra allow six bands of each asymmetric stretching vibrations ν_3 and asymmetric bending vibrations ν_4, two bands of symmetric stretching vibrations ν_1, and four bands of symmetric bending vibrations ν_2. In the IR spectra of $Mn_{0.5}E_2(PO_4)_3$ (E = Ti, Zr) compounds (Fig. 5, spectra *1* and *2*), four or five allowed bands appear in the region of vibrations

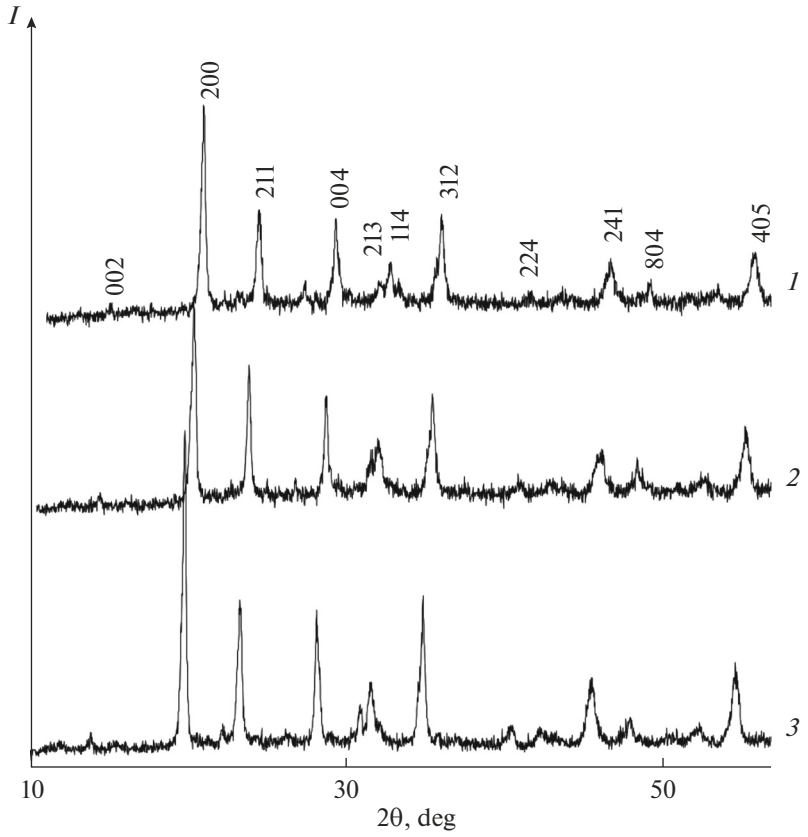

Fig. 4. X-ray diffraction patterns of $Mn_{0.5 + x}Mn_xZr_{2 - x}(PO_4)_3$ phosphates: (*1*) x = 0, (*2*) 0.25, and (*3*) 0.35.

ν_3. The symmetric stretching vibrations ν_1 appear as two bands in the range 990–940 cm^{-1}. Of the six allowed bands ν_4, all the six are observed in the spectra. The vibrations ν_2, detectable by the instrument, appear as two bands.

In the IR spectra of $Mn_{0.5 + 2x}Zr_{2 - x}(PO_4)_3$ solid solutions (Fig. 5, spectra *3* and *4*), the selection rules allow nine of each of the asymmetric stretching vibrations ν_3 and the asymmetric bending vibrations ν_4 of the P–O bond in PO_4^{3-}, three bands of symmetric stretching vibrations ν_1, and six bands of symmetric bending vibrations ν_2 of this ion. The bands in the range 1260–1010 cm^{-1} were assigned to the asymmetric stretching vibrations ν_3 in the PO_4 ion. The high wavenumber values (1258–1215 cm^{-1}) are explained by the fact that, with the large angle POE (E = Ti, Zr) in the structures, the electron density of the polarized E^{4+} ion, which has a small size and a large charge, is partially located at the P–O bond, and this leads to higher values of the force constants of this bond. The bands in the range 970–920 cm^{-1} were assigned to the symmetric stretching vibrations ν_1. The bands in the range 670–550 cm^{-1} correspond to the asymmetric bending vibrations ν_4 of the P–O bond, and the ~430-cm^{-1} bands correspond to the symmetric bending vibrations ν_2 of the P–O bond in PO_4.

In order to verify the structures of the phosphate $Mn_{0.5}Zr_2(PO_4)_3$ and $Mn_{0.5 + x}Mn_xZr_{2 - x}(PO_4)_3$ solid solution with $x = 0.25$ studied in this work, we carried out the Rietveld refinement of their structures at room temperature. The experimental details, unit cell parameters, and selected structure refinement details are compiled in Table 2. Figure 6 shows the measured, calculated, bar, and difference X-ray diffraction patterns for $Mn_{1.0}Zr_{1.75}(PO_4)_3$ ($\equiv Mn_{0.75}Mn_{0.25}Zr_{1.75}(PO_4)_3$). The atomic coordinates, displacement parameters, and occupancy factors for basal atoms of the phosphates are listed in Table 3.

The monoclinic $Mn_{0.5}Zr_2(PO_4)_3$ and $Mn_{1.0}Zr_{1.75}(PO_4)_3$ phases belong to the SW structural type. A fragment of the $Mn_{0.75}Mn_{0.25}Zr_{1.75}(PO_4)_3$ structure is shown in Fig. 7. The basis of the $MnZr_{1.75}(PO_4)_3$ and $Mn_{0.5}Zr_2(PO_4)_3$ structures is the three-dimensional framework $\{Mn_{0.25}Zr_{1.75}(PO_4)_3\}_{3\infty}$ and $\{[Zr_2(PO_4)_3]^-\}_{3\infty}$, respectively, built by linking of octahedra $(Mn,Zr)O_6$ or ZrO_6 and tetrahedra PO_4. Each octahedron shares corners with six tetrahedra PO_4, which are, in turn, each linked with four octahedra. Two (Mn,Zr) or Zr octahedra and three phosphorus-occupied tetrahedra share their corners to form a characteristic fragment of the framework, namely, a "lantern." These groups are packed into zigzag ribbons. Mn^{2+} ions are arranged in framework cavities between the edges of two octahedra, Mn^{2+} ions are arranged with a tetrahedral oxygen coordination (Fig. 7). In $Mn_{0.5}Zr_2(PO_4)$, the zirconium atoms are arranged in a distorted octahedral oxygen surrounding and are disordered over two positions. The Zr–O bond lengths in two independent Zr octahedra are distributed in the ranges 1.75–2.42 and 1.85–2.21 Å, have values typical of six-coordinate zirconium, and the average Zr–O distances in coordination polyhedra are 2.04 and 2.08 Å. In $MnZr_{1.75}(PO_4)_3$, the Mn(Zr)–O distances in mixed octahedra $(Mn,Zr)O_6$ have a greater scatter compared to those in the zirconium–oxygen octahedra in $Mn_{0.5}Zr_2(PO_4)_3$: 1.69–2.43 and 1.81–2.24 Å; the average Mn(Zr)–O distances in coordination polyhedra are close to each other (2.04 and 2.06 Å). The ratios of bond lengths and bond angles in tetrahedra PO_4 in both phosphates are typical of this anion. The tetrahedra are distorted; the average P–O bond lengths in PO_4 polyhedra fall within the range 1.60–1.72 Å. The oxygen surrounding of manganese in extraframework positions may be described as four-coordination: the Mn–O distances to the four nearest-neighboring atoms O fall within the range 1.97–2.85 Å in $Mn_{0.5}Zr_2(PO_4)_3$ and 1.60–2.52 Å in $MnZr_{1.75}(PO_4)_3$.

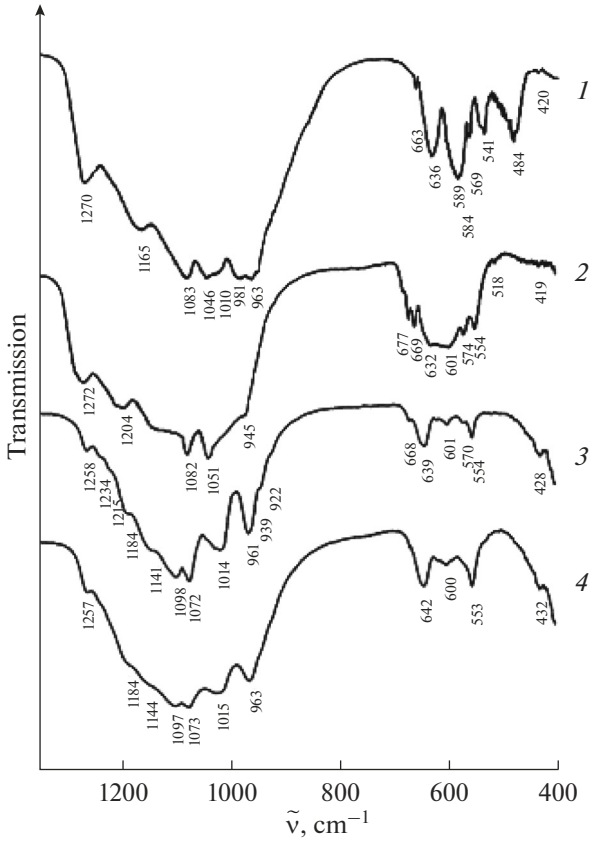

Fig. 5. IR spectra of NZP phosphates: (*1*) $Mn_{0.5}Ti_2(PO_4)_3$ and (*2*) $Mn_{0.5}Zr_2(PO_4)_3$ and those of SW phosphates: $Mn_{0.5 + 2x}Zr_{2 - x}(PO_4)_3$: $x = 0$ (*3*) 0 and (*4*) 0.25.

The prepared $Mn_{0.5}E_2(PO_4)_3$ (E = Ti, Zr) compounds and $Mn_{0.5 + x}Mn_xZr_{2 - x}(PO_4)_3$ ($0 \le x \le 0.35$)

Table 2. Experimental details, unit cell parameters, and selected structure refinement data for phosphates $Mn_{0.5}Zr_2(PO_4)_3$ and $Mn_{1.0}Zr_{1.75}(PO_4)_3$

Parameter	$Mn_{0.5}Zr_2(PO_4)_3$	$Mn_{1.0}Zr_{1.75}(PO_4)_3$
Space group, Z	$P2_1/n$, 4	$P2_1/n$, 4
a, Å	8.861(3)	8.837(4)
b, Å	8.869(2)	8.880(2)
c, Å	12.561(3)	12.595(3)
β, deg	89.51(2)	90.44(3)
V, Å^3	987.1(5)	988.4(5)
ρ_x, g/cm^3	3.330(1)	3.357(1)
2θ angle range, deg	10.00–110.00	10.00–90.00
Scan step	0.02	0.02
Number of reflections	1232	803
Refined parameters:		
structural	59	60
other	19	19
Divergence factors, %:		
R_{wp}	9.14	6.66
R_P	6.68	4.36

solid solution, with their structural similarity (the lantern crystal chemical groups remain unchanged), differ from each other by the way in which manganese cations are positioned in framework cavities: the former belong to space group $P2_1/n$ and Mn occupies tetrahedral cavities in the structure, while the latter belong to space group $R\bar{3}$ and Mn prefers to enter an octahedral surrounding.

The morphotropic transformation can be traced in the series of phosphates of formula unit $M_{0.5}Zr_2(PO_4)_3$

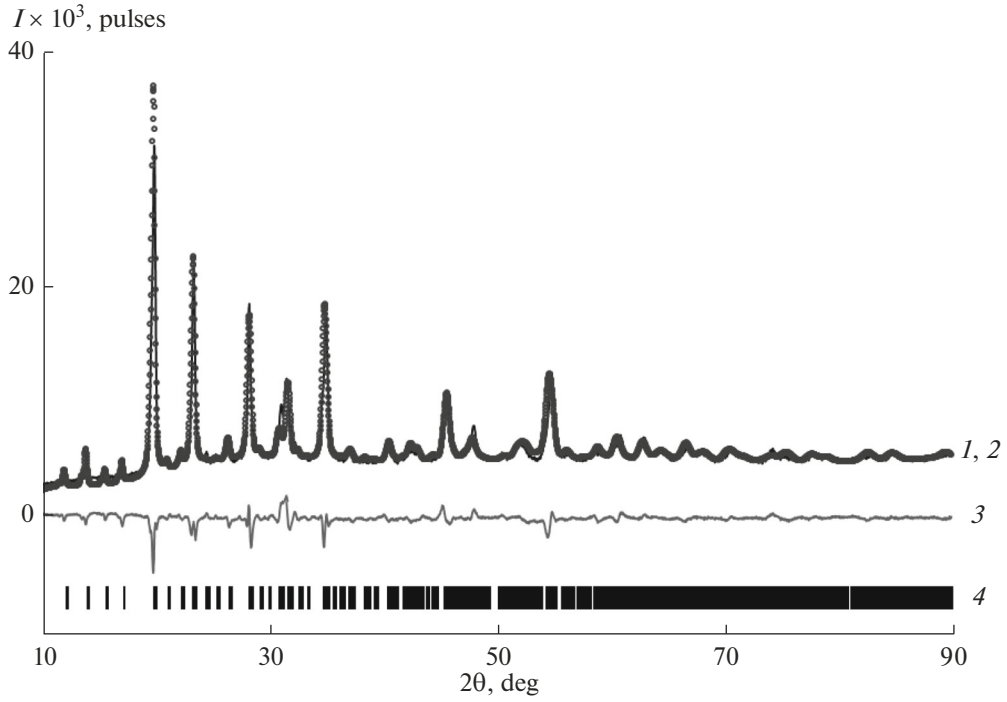

Fig. 6. (*1*) Measured, (*2*) calculated, (*3*) difference, and (*4*) bar X-ray diffraction patterns for $Mn_{1.0}Zr_{1.75}(PO_4)_3$.

Table 3. Atomic coordinates, displacement parameters, and occupancy factors (q) for basal atoms in the structures of $Mn_{0.5}Zr_2(PO_4)_3$ (**I**) and $Mn_{1.0}Zr_{1.75}(PO_4)_3$ ($\equiv Mn_{0.75}Mn_{0.25}Zr_{1.75}(PO_4)_3$) (**II**)

Phosphate	Atom	x	y	z	B_{iso}	q
I	Mn	0.398(6)	0.072(5)	0.335(3)	0.69(6)	0.5
II	Mn(1)	0.364(4)	0.164(4)	0.349(3)		0.75
	Mn(2)	0.766(2)	0.487(1)	0.598(1)		0.125
	Mn(3)	0.736(3)	0.002(2)	0.385(1)		0.125
I	Zr(1)	0.723(2)	0.494(1)	0.601(1)	0.69(6)	1.0
II		0.766(2)	0.487(1)	0.598(1)		0.875
I	Zr(2)	0.760(2)	0.006(1)	0.387(1)	0.69(6)	1.0
II		0.736(3)	0.002(2)	0.385(1)		0.875
I	P(1)	0.606(5)	0.106(5)	0.646(3)	0.69(6)	1.0
II		0.608(6)	0.106(5)	0.645(3)		
I	P(2)	0.629(5)	0.382(5)	0.360(3)	0.69(6)	1.0
II		0.598(5)	0.376(5)	0.347(4)		
I	P(3)	0.033(5)	0.252(6)	0.489(4)	0.69(6)	1.0
II		0.021(5)	0.251(6)	0.490(4)		
I	O(1)	0.648(3)	0.432(2)	0.480(2)	0.69(6)	1.0
II		0.645(3)	0.432(2)	0.479(2)		
I	O(2)	0.683(2)	0.251(2)	0.681(2)	0.69(6)	1.0
II		0.686(2)	0.254(2)	0.684(2)		
I	O(3)	0.936(2)	0.395(2)	0.562(1)	0.69(6)	1.0
II		0.939(2)	0.391(2)	0.565(1)		
I	O(4)	0.568(3)	0.609(3)	0.671(2)	0.69(6)	1.0
II		0.569(3)	0.612(3)	0.675(2)		
I	O(5)	0.831(2)	0.479(2)	0.777(1)	0.69(6)	1.0
II		0.832(2)	0.480(2)	0.773(1)		
I	O(6)	0.837(3)	0.665(2)	0.578(2)	0.69(6)	1.0
II		0.836(3)	0.664(2)	0.579(2)		
I	O(7)	0.687(2)	0.023(2)	0.536(2)	0.69(6)	1.0
II		0.688(2)	0.025(2)	0.532(2)		
I	O(8)	0.660(2)	0.202(2)	0.317(2)	0.69(6)	1.0
II		0.657(2)	0.204(2)	0.315(2)		
I	O(9)	0.907(3)	0.181(2)	0.401(2)	0.69(6)	1.0
II		0.908(3)	0.887(3)	0.406(2)		
I	O(10)	0.571(3)	0.882(3)	0.359(2)	0.69(6)	1.0
II		0.574(3)	0.887(3)	0.356(2)		
I	O(11)	0.790(2)	−0.027(2)	0.214(2)	0.69(6)	1.0
II		0.788(2)	−0.028(2)	0.214(2)		
I	O(12)	0.895(2)	0.852(2)	0.416(2)	0.69(6)	1.0
II		0.895(2)	0.851(2)	0.416(2)		

(where M stands for a metal in the oxidation state +2): Ni (r = 0.55 Å) → Mg (0.57)→ Cu (0.57) →Co (0.58) → Zn (0.60) → Mn (0.66) ↔ Mn (0.83) → Cd (0.95) → Ca (1.00) → Sr (1.18) → Pb (1.19) → Ba (r = 1.35 Å). While in the first half of the series, including $Mn_{0.5}Zr_2(PO_4)_3$ (r_{Mn} = 0.66 Å), metal M has the coordination number equal to four, in the second half, starting with $Mn_{0.5}Zr_2(PO_4)_3$ (r_{Mn} = 0.83 Å), CN_M = 6. Manganese zirconium phosphate, which has two polymorphs, falls at the morphotropic transition boundary in this series. The $Mn_{0.5}Zr_2(PO_4)_3$ polymorphism arises from the easy deformability of oxygen surrounding and the instability of Mn^{2+} coordination, a sufficient flexibility of the construct of corner-sharing Zr and P coordination polyhedra, and the ability of a crystal to more uniformly distribute the stresses arising at large atomic oscillation amplitudes, among various bonds. The phase transition is accompanied by

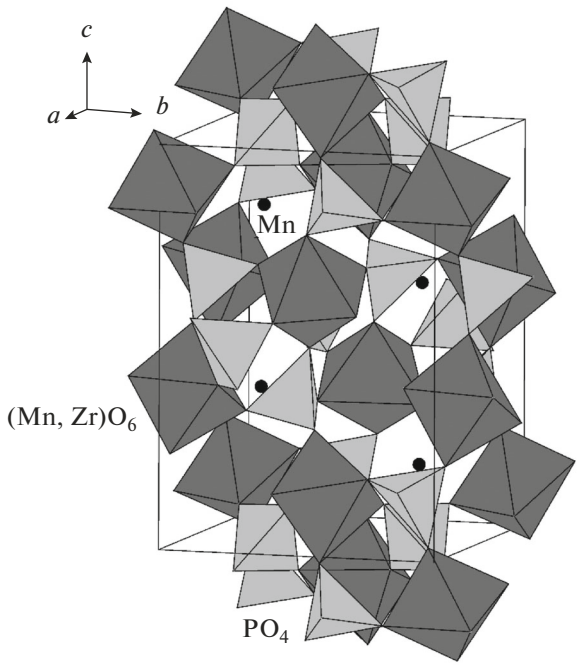

Fig. 7. Fragment of the $Mn_{1.0}Zr_{1.75}(PO_4)_3$ ($\equiv Mn_{0.75}Mn_{0.25}Zr_{1.75}(PO_4)_3$) structure.

rotations of tetrahedra PO_4 and by some modification of the shape of the oxygen surrounding around an Mn atom with the preservation of the general architecture. In the zirconium-phosphate $M_{0.5}Zr_2(PO_4)_3$ morphotropic series, the decisive structure-forming factor in the portion of the series with small cations M^{2+} (compared to Zr^{4+} ions, which are involved in $\{[Zr_2(PO_4)_3]^-\}_{3\infty}$ framework formation), is the octahedral-tetrahedral framework, which is adaptable to a small cation; in the portion of the series with large cations (Cd–Ba), the geometric factor is decisive for atomic arrangement: the arrangement of Zr^{4+} cations compared to the less charged and large ions M^{2+} leads to the "expanding" effect of large MO_6 octahedra on the structure geometry.

CONCLUSIONS

Phase formation has been studied in systems $Mn_{0.5+2x}E_{2-x}(PO_4)_3$ (E = Ti, Zr). Manganese titanium (NZP) and manganese zirconium (SW low-temperature phase and NZP high-temperature phase) double phosphates and $Mn_{0.5+x}[Mn_xZr_{2-x}(PO_4)_3]$ ($0 \le x \le 0.35$) solid solution with the SW structure have been synthesized. The structure has been refined for the low-temperature $Mn_{0.5}Zr_2(PO_4)_3$ phase and the solid solution where manganese atoms occupy framework positions ($CN_{Mn} = 6$) and extraframework positions ($CN_{Mn} = 4$). The basis of the studied phosphate structures has been shown to be a three-dimensional framework built of corner-sharing tetrahedra PO_4 and octahedra ZrO_6 or $(Mn,Zr)O_6$. The effects of various structure-forming factors on structurally related but symmetrically different $M_{0.5}Zr_2(PO_4)_3$ compounds have been discussed.

ACKNOWLEDGMENTS

This study was supported by the Russian Foundation for Basic Research (project no. 15-03-00716_a).

REFERENCES

1. V. I. Pet'kov, A. I. Orlova, G. I. Dorokhova, and Ya. V. Fedotova, Crystallogr. Repts. **45**, 36 (2000).
2. V. I. Pet'kov, V. S. Kurazhkovskaya, A. I. Orlova, and M. L. Spiridonova, Crystallogr. Repts. **47**, 736 (2002).
3. E. A. Asabina, I. O. Glukhova, V. I. Pet'kov, et al., Russ. J. Gen. Chem. **87**, 684 (2017). doi 10.1134/S1070363217040041
4. S. Barth, R. Olazcuaga, P. Gravereau, et al., Mater. Lett. **16**, 96 (1993). https://doi.org/10.1016/0167-577X(93)90031-R.
5. R. Olazcuaga, G. Le Flem, A. Boireau, and J. L. Soubeyroux, Adv. Mater. Res. **1–2**, 177 (1994). https://doi.org/10.4028/www.scientific.net/AMR.1-2.177.
6. V. I. Pet'kov, E. V. Zhilkin, E. A. Asabina, and E. Yu. Borovikova, Russ. J. Inorg. Chem. **59**, 1087 (2014). doi 10.1134/S003602361410012X
7. R. Olazcuaga and J. M. Dance, "Le Flem G. Et Al," J. Solid State Chem. **143**, 224 (1999). https://doi.org/10.1006/jssc.1998.8097.
8. J. Derouet, L. Beaury, P. Porcher, et al., J. Solid State Chem. **143**, 230 (1999). https://doi.org/10.1006/jssc.1998.8098.
9. R. Essehli, B. El Bali, S. Benmokhtar, et al., Mater. Res. Bull. **44**, 1502 (2009). https://doi.org/10.1016/j.materresbull.2009.02.013.
10. M. Schöneborn and R. Glaum, Z. Anorg. Allg. Chem. **634**, 1843 (2008). https://doi.org/10.1002/zaac.200800186.
11. S. Benmokhtar, A. El Jazouli, A. Aatiq, et al., J. Solid State Chem. **180**, 2004 (2007). doi 10.1016/j.jssc.2007.04.014
12. A. Aatiq, M. Menetrier, A. El Jazouli, and C. Delmas, Solid State Ionics **150**, 391 (2002). doi 10.1016/S0167-2738(02)00135-2
13. S. Senbhagaraman, RowT. N. Guru, and A. M. Umarji, J. Mater. Chem. **3**, 309 (1993). doi 10.1039/JM9930300309
14. A. El Bouari and A. El Jazouli, Phosphorus Res. Bull **15**, 136 (2004). doi 10.3363/prb1992.15.0_136
15. D. A. Woodcock, P. Lightfoot, and R. I. Smith, J. Mater. Chem. **9**, 2631 (1999). doi 10.1039/A903489G
16. A. El Jazouli, J. L. Soubeyroux, J. M. Dance, and G. Le Flem, J. Solid State Chem. **65**, 351 (1986). doi 10.1016/0022-4596(86)90107-6
17. J.-P. Chaminade, A. El Bouari, A. El Jazouli, et al., Acta Crystallogr., Sect. A **61**, C325 (2005). doi 10.1107/50108767305086186

18. A. Mouline, M. Alami, R. Brochu, et al., Mater. Res. Bull. **35**, 899 (2000). doi 10.1016/S0025-5408(00)00277-4
19. R. Brochu, M. El-Yacoubi, M. Louer, et al., Mater. Res. Bull. **32**, 15 (1997). doi 10.1016/S0025-5408(96)00162-6
20. J. Alamo and J. L. Rodrigo, Solid State Ionics **63–65**, 678 (1993). doi 10.1016/0167-2738(93)90178-6
21. A. El Yacoubi, A. Mouline, M. Alami, et al., Phys. Chem. News **44**, 76 (2008).
22. E. R. Gobechiya, Yu. K. Kabalov, V. I. Pet'kov, and M. V. Sukhanov, Crystallorg. Repts. **49**, 741 (2004).
23. V. I. Pet'kov, A. I. Orlova, and D. A. Kapranov, Russ. J. Inorg. Chem. **43**, 1429 (1998).
24. V. I. Petkov and A. I. Orlova, J. Therm. Anal. Calom. **54**, 71 (1998). https://doi.org/10.1023/A:1010156616525.
25. M. Kinoshita, A. N. Fitch, Y. Piffard, et al., Eur. J. Solid State Inorg. Chem. **28**, 683 (1991).
26. E. R. Gobechiya, M. V. Sukhanov, V. I. Pet'kov, and Yu. K. Kabalov, Crystallorg. Repts. **53**, 53 (2008). doi 10.1134/S1063774508010069
27. A. El Jazouli, M. Alami, R. Brochu, et al., J. Solid State Chem. **71**, 444 (1987). doi 10.1016/0022-4596(87)90253-2
28. K. Nomura, S. Ikeda, H. Masuda, and H. Einaga, Solid Electrolyte. Chem. Lett. **22**, 893 (1993). doi 10.1246/cl.1993.893
29. K. Nomura, S. Ikeda, K. Ito, and H. Einaga, Bull. Chem. Soc. Jpn. **65**, 3221 (1992). https://doi.org/10.1246/bcsj.65.3221.
30. V. I. Pet'kov, A. I. Orlova, G. N. Kazantsev, et al., J. Therm. Anal. Calom. **66**, 623 (2001). https://doi.org/10.1023/A:1013145807987.
31. V. Pet'kov, E. Asabina, V. Loshkarev, and M. Sukhanov, J. Nucl. Mater. **471**, 122 (2016). doi 10.1016/j.jnucmat.2016.01.016
32. S. N. Ienealem, S. G. Gul'yanova, T. K. Chekhlova, et al., Zh. Fiz. Khim. **74**, 2273 (2000).
33. M. Sukhanov, V. Pet'kov, M. Ermilova, et al., Phosphorus Res. Bull. **19**, 90 (2005). https://doi.org/10.3363/prb1992.19.0_90.
34. I. Shchelokov, E. Asabina, M. Sukhanov, et al., Solid State Sci. **10**, 513 (2008). doi 10.1016/j.solidstatesciences.2007.12.005
35. A. I. Pylinina, I. I. Mikhalenko, M. M. Ermilova, et al., Russ. J. Phys. Chem. A. **84**, 400 (2010). doi 10.1134/S0036024410030106
36. H. M. Rietveld, Acta Crystallogr. **22**, 151 (1967).
37. Y. I. Kim and F. Izumi, J. Ceram. Soc. Jpn. **102**, 401 (1994). doi 10.2109/jcersj.102.401
38. F. Izumi, *The Rietveld Method*, Ed. by C. A. Young (Oxford Univ. Press, Oxford, 1993).
39. V. I. Pet'kov, M. V. Sukhanov, A. S. Shipilov, et al., Inorg. Mater. **50**, 263 (2014). doi 10.1134/S0020168514030091

Translated by O. Fedorova